AIP Applied Physics Letters

Multifunctional semiconductor micro-Hall devices for magnetic, electric, and photo-detection

A. M. Gilbertson, Hatef Sadeghi, V. Panchal, O. Kazakova, C. J. Lambert, S. A. Solin, and L. F. Cohen

Citation: Applied Physics Letters **107**, 233504 (2015); doi: 10.1063/1.4936932
View online: http://dx.doi.org/10.1063/1.4936932
View Table of Contents: http://scitation.aip.org/content/aip/journal/apl/107/23?ver=pdfcov
Published by the AIP Publishing

Articles you may be interested in
Three-axis Hall transducer based on semiconductor microtubes
Appl. Phys. Lett. **103**, 173513 (2013); 10.1063/1.4826680

Micro-Hall position sensing of magnetic nanowires
J. Appl. Phys. **106**, 074518 (2009); 10.1063/1.3245334

Highly sensitive micro-Hall devices based on Al 0.12 In 0.88 Sb/In Sb heterostructures
J. Appl. Phys. **98**, 014506 (2005); 10.1063/1.1954867

Generation–recombination noise in doped-channel Al 0.3 Ga 0.7 As/GaAs/In 0.2 Ga 0.8 As quantum well micro-Hall devices
J. Appl. Phys. **94**, 7590 (2003); 10.1063/1.1625783

InAs/Al 0.2 Ga 0.8 Sb quantum well Hall sensors with improved temperature stability
Rev. Sci. Instrum. **70**, 2715 (1999); 10.1063/1.1149834

This article is copyrighted as indicated in the article. Reuse of AIP content is subject to the terms at: http://scitation.aip.org/termsconditions. Downloaded to IP: 148.88.176.132 On: Mon, 14 Dec 2015 11:14:40

APPLIED PHYSICS LETTERS **107**, 233504 (2015)

Multifunctional semiconductor micro-Hall devices for magnetic, electric, and photo-detection

A. M. Gilbertson,[1] Hatef Sadeghi,[2] V. Panchal,[3] O. Kazakova,[3] C. J. Lambert,[2] S. A. Solin,[1,4] and L. F. Cohen[1]
[1]*Blackett Laboratory, Imperial College London, Prince Consort Road, London SW7 2BZ, United Kingdom*
[2]*Department of Physics, Lancaster University, Lancaster LA1 4YB, United Kingdom*
[3]*National Physical Laboratory, Teddington TW11 0LW, United Kingdom*
[4]*Department of Physics and Institute for Materials Science and Engineering, Washington University in St. Louis, St. Louis, Missouri 63130, USA*

(Received 11 July 2015; accepted 20 November 2015; published online 9 December 2015)

We report the real-space voltage response of InSb/AlInSb micro-Hall devices to local photo-excitation, electric, and magnetic fields at room temperature using scanning probe microscopy. We show that the ultrafast generation of localised photocarriers results in conductance perturbations analogous to those produced by local electric fields. Experimental results are in good agreement with tight-binding transport calculations in the diffusive regime. The magnetic, photo, and charge sensitivity of a 2 μm wide probe are evaluated at a 10 μA bias current in the Johnson noise limit (valid at measurement frequencies > 10 kHz) to be, respectively, 500 nT/$\sqrt{}$Hz; 20 pW/$\sqrt{}$Hz ($\lambda = 635$ nm) comparable to commercial photoconductive detectors; and 0.05 $e/\sqrt{}$Hz comparable to that of single electron transistors. These results demonstrate the remarkably versatile sensing attributes of simple semiconductor micro-Hall devices that can be applied to a host of imaging and sensing applications. © *2015 AIP Publishing LLC*. [http://dx.doi.org/10.1063/1.4936932]

Multifunctional mesoscopic sensors capable of detecting local magnetic, electric, and optical fields can greatly facilitate image capture in nano-arrays that address a multitude of disciplines spanning information storage to medical biosensing. While the magnetic sensing attributes of micro-Hall devices based on high mobility 2D electron gas (2DEG) systems are well known,[1,2] the sensitivity of the transverse voltage output to local electric fields (in zero magnetic field) has only recently been investigated and shows the capability for detecting single electron charges.[3–5] In this letter, we study the real-space voltage response and sensitivity of InSb 2DEG micro-Hall devices to local electric (E) field, magnetic (B) field and photo-excitation, at room temperature (RT) using electrical and magnetic scanning gate microscopy (SGM) and scanning photovoltage microscopy (SPVM), respectively. SGM and SPVM have been used by numerous groups to study local transport phenomena in buried semiconductor 2DEG nanostructures. In particular, the high spatial resolution afforded by the SGM technique has been successfully applied to visualise coherent electron flow from quantum point contacts.[6,7] Meanwhile, SPVM experiments have focused primarily on the quantum Hall regime to visualise edge channel transport at the sample boundaries.[8,9] Recently, SPVM has been used to image ballistic photocurrents,[10] spin-dependent transverse photovoltages,[11] and metal-semiconductor interface effects[12,13] in GaAs-based microstructures. Meanwhile, InSb 2DEG structures are particularly well suited to sensing applications due to the high RT electron mobility[14,15] of $\mu_e < 60\,000\,\mathrm{cm^2/V\,s}$, exceeded only by that in suspended/encapsulated graphene.[16] Here, we show that micro-Hall devices exhibit a distinctive photoresponse analogous to their E-field response, due to the equivalence of the local conductivity perturbations on the current distribution in the vicinity of voltage leads. Experimental results are well described by calculations in the diffusive transport regime. In addition to exhibiting excellent magnetic sensitivity, we demonstrate that micro-Hall devices exhibit a remarkable charge and photo-sensitivity. These results demonstrate the versatile multifunctional sensing attributes of the simplest 2DEG Hall devices.

The samples studied are fabricated from a modulation doped InSb/$Al_xIn_{1-x}Sb$ quantum well (QW) heterostructure grown by molecular beam epitaxy on a semi-insulating GaAs (001) substrate. The 2DEG is located in a 15 nm thick InSb QW buried 50 nm beneath the surface with an $Al_{0.2}In_{0.8}Sb$ top cap. Further details of the layer structure are given elsewhere.[17] Micro-Hall cross structures with lateral dimensions (w) varying between 1 μm and 4 μm were fabricated using e-beam lithography and shallow (≈150 nm etch depth) reactive ion etching in a CH_4/H_2 gas mixture. Cr/Au Ohmic contacts to the InSb 2DEG were formed using a subtractive etch technique.[17] Here, we focus on the results from a $w = 2\,\mu$m Hall cross structure (SPVM and SGM data from a 1 μm and 4 μm device are presented in the supplementary material[18]). The RT electrical transport properties of the devices are characterised by an electron density $n_0 = 5 \times 10^{11}\,\mathrm{cm^{-2}}$, $\mu_e = 34\,000\,\mathrm{cm^2/V\,s}$, and resistivity $\rho_0 = 367\ \Omega/\square$, as determined by conventional magnetotransport measurements.

All measurements presented were performed at RT under ambient conditions with a constant DC bias current I_0 applied across the device. In the SPVM measurement, samples are optically excited using a $\lambda = 635$ nm *cw* diode laser. The light is mechanically chopped at 512 Hz and focused onto the sample surface through a microscope objective yielding a spot diameter of ≈0.5 μm. The sample position (x,y) is raster scanned with respect to the laser spot and the resulting photo-induced longitudinal, ΔV_{xx}(x,y), and transverse, ΔV_{xy}(x,y), voltages [see Fig. 1(c)] are recorded using a

 © 2015 AIP Publishing LLC

This article is copyrighted as indicated in the article. Reuse of AIP content is subject to the terms at: http://scitation.aip.org/termsconditions. Downloaded to IP: 148.88.176.132 On: Mon, 14 Dec 2015 11:14:40

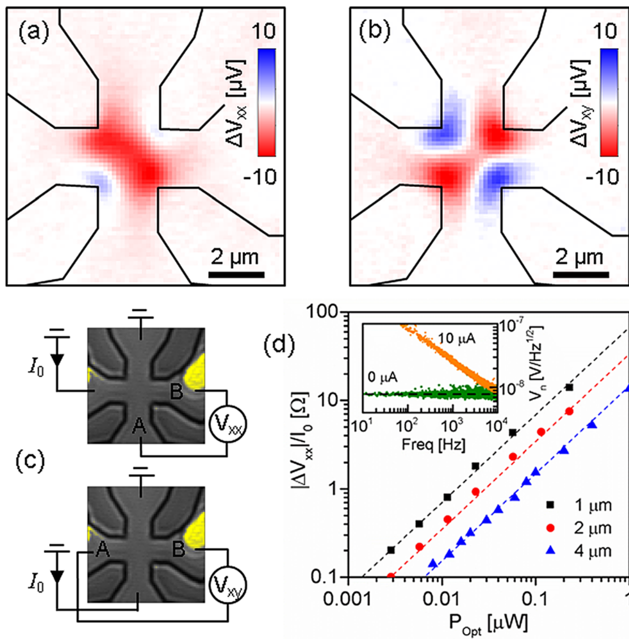

FIG. 1. (a) and (b) SPVM images of ΔV_{xx} and ΔV_{xy} from a 2 μm InSb 2DEG micro-Hall device. The outline of the device is shown by the black lines ($I_0 = 10$ μA; $P_{opt} = 20$ nW). (c) Optical reflection images showing the measurement configurations. (d) Dependence of $|\Delta V_{xx}|/I_0$ on P_{Opt} for different sized devices, obtained from the centre of the cross. Dashed lines are a guide to the eye indicating a linear dependence. Inset shows voltage noise spectra from the 2 μm device.

standard lock-in technique. The reflected light intensity from the sample surface is acquired simultaneously using a Si avalanche photodiode in order to correlate the photovoltage signals with the device geometry. The local *E*-field response of the device was investigated using an electrical SGM technique based on non-contact mode atomic force microscopy (AFM). During the AFM scan, an AC voltage, V_{Tip} (at f_{Tip} $= 2.5$ kHz), is applied between a non-magnetic PtIr-coated AFM tip (AppNano ANSCM-PA, radius $r = 30$ nm) and the 2DEG. The tip is held at a lift height of $h = 20$ nm above the sample surface. The surface is scanned and the resulting tip-induced voltages ΔV_{xx}(x, y) and ΔV_{xy}(x, y) are recorded using a lock-in amplifier referenced to f_{Tip}. The local *B*-field response was investigated by magnetic SGM with a Co-coated AFM tip (NANOSENSORS™ PPP-MFMR, $r < 30$ nm) utilising the Kelvin probe feedback mode to compensate the electrostatic contributions.[19] In this case, the device experiences a local AC magnetic field produced by the mechanical oscillation of the tip at $f_0 = 75$ kHz, and ΔV_{xx}(x, y) and ΔV_{xy} (x, y) maps are recorded using a lock-in amplifier referenced to f_0.

Figures 1(a) and 1(b) show the longitudinal and transverse SPVM images from the 2 μm micro-Hall device obtained with an incident optical power $P_{Opt} = 20$ nW. Optical reflection images of the device illustrating the measurement configurations are shown in Fig. 1(c). The spatial dependence of the photovoltages exhibits distinctive symmetries: ΔV_{xx}(x, y) is characterised by a band of negative photovoltage extending across the diagonal of the active area, between adjacent current and voltage leads [see Fig. 1(a)]. In contrast, ΔV_{xy} (x, y) exhibits a two-fold symmetry characterised by photovoltage of alternating polarity when the laser spot is located at each corner of the cross junction [see Fig. 1(b)]. Local photoexcitation generates a steady-state photocarrier density $\Delta n \propto P_{Opt}$ subject to carrier drift and diffusion (the contribution from holes can be ignored due to their relatively low mobility $\mu_h \sim \mu_e/100$).[20] The relative contributions of the drift and diffusion components to the photovoltage signal vary with P_{Opt} and I_0. For the low excitation powers used here, no photoresponse is observed for $I_0 = 0$, indicating negligible contributions from diffusion and photovoltaic[21] effects. The observed photoresponse for $I_0 \neq 0$ is therefore dominated by the drift of photocarriers in the applied *E*-field. Accordingly, we find the photovoltage is proportional to I_0 and exhibits a linear dependence on P_{opt} over several orders of magnitude, confirming the photoconductive origin of the photoresponse:[18] results from different sized devices are summarised in Fig. 1(d). To quantify the photosensitivity, we determine the noise-equivalent power (*NEP*) according to $NEP = V_n/R_{ph}$, where $R_{ph} = \Delta V_{xx}/\Delta P_{opt}$ is the photoresponsivity and V_n is the rms voltage noise per unit bandwidth. Measured noise spectra from the 2 μm device with $I_0 = 0$ and 10 μA applied are shown in the inset to Fig. 1(d). For frequencies >10 kHz beyond the 1/*f* corner frequency, in the so-called Johnson noise limit (JNL), V_n is equal to the thermal voltage noise, $V_{th} = \sqrt{4k_BTR_{2t}}$, shown by dashed line which sets a lower bound for the corresponding sensitivity (k_B is the Boltzman constant, $T = 295$ K is the temperature, and $R_{2t} = 4$ kΩ is the two-terminal output resistance of the device). For consistency sensitivities are quoted in the JNL for the remainder of the paper. For the 2 μm device with $R_{ph} = 400$ V/W at a 10 μA bias current, the *NEP* is ≈20 pW/$\sqrt{}$Hz, which is comparable to commercial photodiodes (InGaAs and Ge) and photoconductive detectors (PbSe).[22]

Additional measurements were performed on a 40 μm wide Hall-bar with $P_{Opt} = 4$ μW, as shown schematically in Fig. 2(a). This larger sample represents an "open" system in which the mesa boundaries and adjacent voltage leads are well separated, allowing us to examine the photoresponse near an individual voltage lead. Fig. 2(b) shows the ΔV_{xx}(x,y) image obtained in the vicinity of voltage lead A. The photoresponse is characterised by two signal lobes of opposite polarity emanating from the voltage lead entrance. The corresponding photovoltage map of lead B is reversed due to the differential (A-B) measurement [see Fig. 2(a)]. To interpret these results, we note that close to the voltage lead

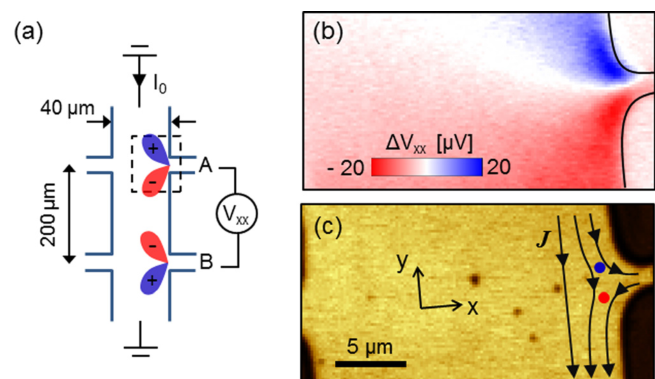

FIG. 2. (a) Schematic of the macroscopic Hall-bar and measurement geometry; the dashed box indicates the scanned area; coloured lobes represent the observed photovoltage signals. (b) SPVM image of ΔV_{xx} in the vicinity of a voltage lead A ($I_0 = 100$ μA; $P_{Opt} = 4$ μW). (c) Optical reflection image with a sketch of the current lines near the voltage lead.

This article is copyrighted as indicated in the article. Reuse of AIP content is subject to the terms at: http://scitation.aip.org/termsconditions. Downloaded to IP: 148.88.176.132 On: Mon, 14 Dec 2015 11:14:40

entrance, the transverse current density J_x is non-zero and changes direction, as shown by the sketched current lines in Fig. 2(c). Photocarriers generated above (below) the voltage lead [blue (red) dot in Fig. 2(c)] undergo net drift towards (away from) the lead thereby causing its potential to adjust in order to satisfy $J_x = 0$ in the lead. With knowledge of the photoresponse of an individual voltage lead, construction of both the ΔV_{xx}(x,y) and ΔV_{xy}(x,y) patterns observed in the "closed" Hall cross geometry is straightforward by considering the location of the second voltage lead and the relative current direction. The SPVM images therefore reveal important information about the local *E*-field distribution in the device.

Next, we discuss the response of the device to local *E*-fields generated from an electrically biased metallic SPM-AFM tip (see experimental section). Figs. 3(a) and 3(b) show electrical SGM images of the ΔV_{xx}(x,y) and ΔV_{xy}(x,y) voltage outputs from the 2 μm device, obtained with $V_{Tip} = 3.5$ V (rms). It is immediately evident that the general features observed in the SPVM images are reproduced in the SGM images. Similar results are found for the 1 μm and 4 μm devices.[18] The SGM images are similar to those reported previously[3,23] and can be understood by considering the effect of the local tip-induced potential well/barrier on the current flow near the voltage leads in a similar way to the discussion of the SPVM images. Here, the charged tip alters the electron density Δn beneath the tip via capacitive coupling to the 2DEG. Because the conductivity modulation $\Delta\sigma = \Delta n e \mu_e$ is in-phase with the AC tip voltage, $\Delta\sigma > 0$ as for the photoconductive response. After taking into account the fraction ($2\pi r^2/w^2$) of charge carriers interacting with the tip, it is straightforward to show that $\Delta\sigma = \mu_e C V_{Tip}/w^2$, where C is the tip-2DEG capacitance. The inset to Fig. 4 shows the linear dependence of ΔV_{xx} on V_{Tip} from different sized devices, obtained from the centre of the cross. To accurately determine the sensitivity of the device to electric charge induced on the tip, $Q_{Tip} = CV_{Tip}$, calculation of the electrostatic potential around the metallic tip is required which is beyond the scope of this work. For simplicity, we model the tip as a sphere of radius $r = 30$ nm separated from

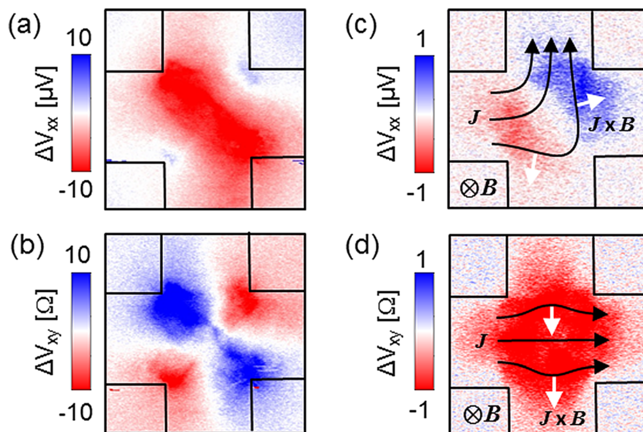

FIG. 3. (a) and (b) Electrical SGM images of ΔV_{xx} and ΔV_{xy} from the 2 μm device ($V_{Tip} = 3.53$ V, $I_0 = 10$ μA). (c) and (d) Magnetic SGM images of ΔV_{xx} and ΔV_{xy} (tip magnetisation into the page); the current flow and direction of Lorentz force are shown schematically by the black and white arrows, respectively.

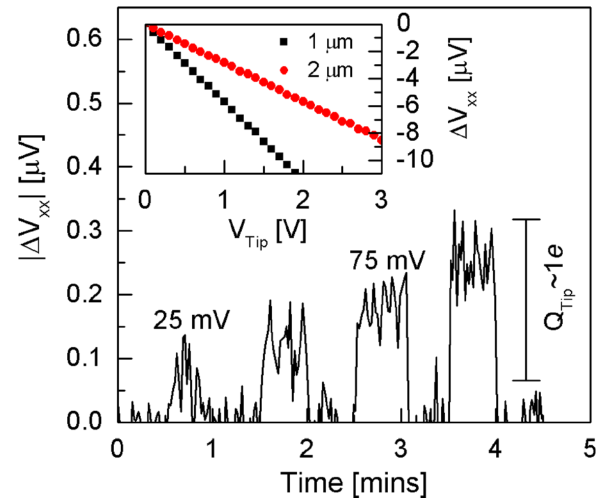

FIG. 4. Changes in ΔV_{xx} from the 2 μm device caused by small voltages applied to the tip in a step-wise manner (25 mV increments). Inset shows the linear dependence of ΔV_{xx} on V_{Tip} for different sized devices, obtained from the centre of the cross. ($I_0 = 10$ μA, $f_{Tip} = 2.5$ kHz).

the 2DEG by $(h + t)$, where t is the $Al_{0.2}In_{0.8}Sb$ cap thickness. The tip-2DEG capacitance is then given by $C = 2\pi\varepsilon_0\varepsilon_r r^2/(h\varepsilon_r + t)$, where ε_0 is the permittivity of free space and $\varepsilon_r \approx 16$ is the relative permittivity of $Al_{0.2}In_{0.8}Sb$ (estimated using Vegard's rule for the ternary system[24,25] with $\varepsilon_r(x) \approx 16.8$–$5.6x$). Due to the small tip radius, coupling to the 2DEG is rather weak, yielding $C \approx 2$ aF. To test the validity of this model, we can estimate ΔV_{xx} when the tip is in the cross centre through the relation $\Delta V_{xx} = I_0 \Delta R$, where $\Delta R \cong -\frac{L}{w}\rho_0^2\Delta\sigma$. For a 2 μm device with $w \approx L$, $V_{Tip} = 3.5$ V, and $I_0 = 10$ μA, this simple model for the tip-2DEG interaction yields $\Delta V_{xx} \approx -10$ μV, which is in good agreement with the experimental data. Proceeding with the analysis, we deduce a charge responsity for the 2 μm device of $R_Q = \Delta V_{xx}/\Delta Q_{Tip} \approx 240$ nV/e at a 10 μA bias current and a charge sensitivity of $V_{th}/R_Q \approx 0.05$ $e/\sqrt{\text{Hz}}$. This sensitivity is significantly greater than that of the previous reports of 2DEG Hall cross structures[3] and is comparable to the best reported single-electron transistor sensitivity at RT.[26] Sensitivities derived for the 1 and 4 μm devices are given in the supplementary material.[18] To demonstrate the sensitivity to small *E*-fields, in Fig. 4 we show the measured changes in ΔV_{xx} caused by small tip voltages corresponding to $Q_{Tip} \ll 1e$ applied in a step-wise manner. We note that the rms voltage noise for the data in Fig. 4 is $\approx$25 nV with the effective measurement bandwidth of 0.42 Hz. This corresponds to $V_n \approx 35$ nV/$\sqrt{\text{Hz}}$ and a charge sensitivity of $\approx$0.15 $e/\sqrt{\text{Hz}}$, in line with the expected sensitivity in the JNL. These results demonstrate that $\ll 1e$ charge resolution is readily achieved in the current micro-Hall device.

For completeness, in Figs. 3(c) and 3(d), we show the magnetic SGM images for ΔV_{xx}(x,y) and ΔV_{xy}(x,y) (tip magnetisation into the page). Here, ΔV_{xy}(x, y) represents the local Hall response [Fig. 3(d)], characterised by a rotationally symmetric signal in the centre of the cross, consistent with the previous magnetic SGM experiments on graphene[19,27,28] and InAs 2DEG[5] Hall probes. ΔV_{xx}(x, y) represents the local magnetoresistance of the device and displays a distinct asymmetry about the line bisecting the adjacent current and voltage leads [Fig. 3(c)]. The symmetry of both

This article is copyrighted as indicated in the article. Reuse of AIP content is subject to the terms at: http://scitation.aip.org/termsconditions. Downloaded to IP: 148.88.176.132 On: Mon, 14 Dec 2015 11:14:40

ΔV_{xx}(x,y) and ΔV_{xy}(x,y) follow from the direction of the local Lorentz force (**J × B**) exerted on the 2DEG by the magnetic tip [see Figs. 3(c) and 3(d)]. Using the measured Hall coefficient $R_H = 1/n_0 e = 1.25\,\mathrm{k}\Omega/\mathrm{T}$, we deduce a magnetic sensitivity of $V_{th}/I_0 R_H \approx 500\ \mathrm{nT}/\sqrt{\mathrm{Hz}}$ at 10 μA. This sensitivity greatly exceeds that of chemical vapour deposited[29] and epitaxial[30] graphene Hall probes and is comparable to the previous Sb-based 2DEG[31] Hall probes with comparable dimensions and bias current.

To model the spatial response of the micro-Hall device to a local non-magnetic conductance perturbation, we consider the four-probe tight-binding lattice shown in Fig. 5(a) consisting of 4 crystalline leads labelled 1, 2, 3, and 4 (white regions) connected to a square scattering region (light grey and blue region) to which we introduce disorder. The Hamiltonian matrix elements H_{ij} are chosen to be $-\gamma$ for i,j nearest neighbours, and onsite energies H_{ii} are chosen to be zero in the leads. Electrons travelling from one lead to another can possess energies between -4γ and 4γ, where -4γ corresponds to the conduction band edge. Within the scattering region diagonal elements are chosen to be $H_{ii} = \varepsilon_i + f(\underline{r_i} - \underline{r})$, where ε_i is the onsite energy in site i. To simulate a diffusive scatterer, ε_i is a random number uniformly distributed over the interval $[-W, W]\ \gamma$. In the simulation, the width of disorder W is chosen to be 0.8 and the average conductance is obtained by averaging over an ensemble of 100 samples. For such disorder with the chosen sample size of 82×82 lattice sites, the system exhibits Ohmic behaviour, where the conductivity is approximately independent of length. For this choice of parameters, the mean free path of the electrons is $\approx 40a$ obtained by the method described in Ref. 32.To simulate a local conductance perturbation, we introduce a local electrostatic potential inhomogeneity centred on site i, $f(\underline{r_i} - \underline{r})$ with a Gaussian distribution of radius $5a$ (a is the lattice constant) and maximum value of $-\gamma$. The four-probe resistance is calculated using Landauer-Büttiker formalism[33] as the position of the potential inhomogeneity is varied. Using the numbering convention shown in Fig. 5(a), the transverse and longitudinal resistances are $R_{xy} = A^{-1}_{32} - A^{-1}_{34}$ and $R_{xx} = A^{-1}_{42} - A^{-1}_{43}$, where $A_{ij} = N_i \delta_{ij} - T_{ij}$ and $i, j \in [1, 2, 3]$. N_i is the number of open conduction channels in lead i and T_{ij} is the transmission coefficient between lead i and j calculated using the Gollum quantum transport method[32] as described in Refs. 34 and 35.

Figures 5(b) and 5(c) show the calculated $\Delta R_{xx}(x,y) = R_{xx}(x,y) - R_{xx0}$ and $\Delta R_{xy}(x,y) = R_{xy}(x,y) - R_{xy0}$ maps for the diffusive regime at a Fermi energy $E_F = -2\gamma = -2$, where R_{xx0} and R_{xy0} are the resistances without the potential inhomogeneity. Here, E_F is chosen to be sufficiently small to ensure an approximately circular Fermi surface. The band structure is then approximately $E = -4\gamma + \gamma(k_x^2 + k_y^2)/2$. This yields a Fermi wavelength of $\lambda_F \approx \pi a$. As evidenced by comparing Fig. 5 with Figs. 1 and 3, the numerical calculations reproduce well the salient features observed in the experimental SPVM and electrical SGM data, validating our approach and interpretation.

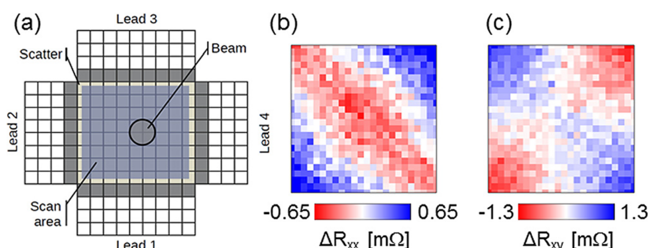

FIG. 5. (a) Schematic diagram of the calculated structure. Calculated (b) ΔR_{xx} and (c) ΔR_{xy} maps in the 82×82 site scattering region.

In summary, the real-space voltage response of InSb 2DEG micro-Hall devices to local photo-excitation, electric and magnetic fields have been studied at room temperature using scanning probe techniques. Local photoexcitation is demonstrated to have an analogous effect on the electric field distribution in the 2DEG to that of a local electrostatic gate. In addition to exhibiting high magnetic field sensitivity, we demonstrate that micro-Hall devices exhibit a photosensitivity comparable to commercial photoconductive sensors and a remarkable sub $1e$ charge resolution, equal to the best single electron transistor reports at room temperature.

The authors gratefully acknowledge funding from the EPSRC (EP/J014699/1). S.A.S. has also been supported by the NSF (ECCS-0725538) and is a co-founder of PixelEXX, a start-up company whose mission is to market imaging arrays.

[1] G. Boero, M. Demierre, P. A. Besse, and R. S. Popovic, "Micro-Hall devices: Performance, technologies and applications," Sens. Actuators, A **106**(1–3), 314–320 (2003).
[2] J. Lenz and A. S. Edelstein, "Magnetic sensors and their applications," IEEE Sens. J. **6**(3), 631–649 (2006).
[3] I. I. Barbolina, K. S. Novoselov, S. V. Morozov, S. V. Dubonos, M. Missous, A. O. Volkov, D. A. Christian, I. V. Grigorieva, and A. K. Geim, "Submicron sensors of local electric field with single–electron resolution at room temperature," Appl. Phys. Lett. **88**(1), 013901 (2006).
[4] A. Baumgartner, T. Ihn, K. Ensslin, G. Papp, F. Peeters, K. Maranowski, and A. C. Gossard, "Classical Hall effect in scanning gate experiments," Phys. Rev. B **74**(16), 165426 (2006).
[5] L. Folks, A. S. Troup, T. D. Boone, J. A. Katine, M. Nishioka, M. Grobis, G. J. Sullivan, A. Ikhlassi, M. Field, and B. A. Gurney, "Near-surface nanoscale InAs Hall cross sensitivity to localized magnetic and electric fields," J. Phys.-Condens. Matter **21**(25), 255802 (2009).
[6] M. A. Topinka, B. J. Leroy, R. M. Westervelt, K. D. Maranowski, and A. C. Gossard, "Imaging coherent electron wave flow in a two-dimensional electron gas," Physica E **12**(1–4), 678–683 (2002).
[7] K. E. Aidala, R. E. Parrott, T. Kramer, E. J. Heller, R. M. Westervelt, M. P. Hanson, and A. C. Gossard, "Imaging magnetic focusing of coherent electron waves," Nat. Phys. **3**(7), 464–468 (2007).
[8] A. A. Shashkin, A. J. Kent, J. R. Owers-Bradley, A. J. Cross, P. Hawker, and M. Henini, "Hall photovoltage imaging of the edge of a quantum Hall device," Phys. Rev. Lett. **79**(25), 5114–5117 (1997).
[9] R. J. F. vanHaren, W. deLange, F. A. P. Blom, and J. H. Wolter, "Imaging of edge channels in the integer quantum Hall regime by the lateral photoelectric effect," Phys. Rev. B **52**(8), 5760–5766 (1995).
[10] K. D. Hof, F. J. Kaiser, M. Stallhofer, D. Schuh, W. Wegscheider, P. Hanggi, S. Kohler, J. P. Kotthaus, and A. W. Holleitner, "Spatially resolved ballistic optoelectronic transport measured by quantized photocurrent spectroscopy," Nano Lett. **10**(10), 3836–3840 (2010).
[11] L. Nadvornik, J. A. Haigh, K. Olejnik, A. C. Irvine, V. Novak, T. Jungwirth, and J. Wunderlich, "Efficient conversion of light to charge and spin in Hall-bar microdevices," Phys. Rev. B **91**(12), 125205 (2015).
[12] A. K. M. Newaz, W. J. Chang, K. D. Wallace, L. C. Edge, S. A. Wickline, R. Bashir, A. M. Gilbertson, L. F. Cohen, and S. A. Solin, "A nanoscale Ti/GaAs metal-semiconductor hybrid sensor for room temperature light detection," Appl. Phys. Lett. **97**(8), 082105 (2010).
[13] L. C. Tran, F. M. Werner, A. K. M. Newaz, and S. A. Solin, "Photo effects at the Schottky interface in extraordinary optoconductance," J. Appl. Phys. **114**(15), 153110 (2013).

This article is copyrighted as indicated in the article. Reuse of AIP content is subject to the terms at: http://scitation.aip.org/termsconditions. Downloaded to IP: 148.88.176.132 On: Mon, 14 Dec 2015 11:14:40

[14] J. M. S. Orr, A. M. Gilbertson, M. Fearn, O. W. Croad, C. J. Storey, L. Buckle, M. T. Emeny, P. D. Buckle, and T. Ashley, "Electronic transport in modulation-doped InSb quantum well heterostructures," Phys. Rev. B **77**(16), 165334 (2008).
[15] A. M. Gilbertson, A. Kormanyos, P. D. Buckle, M. Fearn, T. Ashley, C. J. Lambert, S. A. Solin, and L. F. Cohen, "Room temperature ballistic transport in InSb quantum well nanodevices," Appl. Phys. Lett. **99**(24), 242101 (2011).
[16] L. Wang, I. Meric, P. Y. Huang, Q. Gao, Y. Gao, H. Tran, T. Taniguchi, K. Watanabe, L. M. Campos, D. A. Muller, J. Guo, P. Kim, J. Hone, K. L. Shepard, and C. R. Dean, "One-dimensional electrical contact to a two-dimensional material," Science **342**(6158), 614–617 (2013).
[17] A. M. Gilbertson, P. D. Buckle, M. T. Emeny, T. Ashley, and L. F. Cohen, "Suppression of the parasitic buffer layer conductance in InSb/AlxIn1-xSb heterostructures using a wide-band-gap barrier layer," Phys. Rev. B **84**(7), 075474 (2011).
[18] See supplementary material at http://dx.doi.org/10.1063/1.4936932 for additional information and data from devices.
[19] V. Panchal, O. Iglesias-Freire, A. Lartsev, R. Yakimova, A. Asenjo, and O. Kazakova, "Magnetic scanning probe calibration using graphene Hall sensor," IEEE Trans. Magn. **49**(7), 3520–3523 (2013).
[20] P. Gu, M. Tani, S. Kono, K. Sakai, and X. C. Zhang, "Study of terahertz radiation from InAs and InSb," J. Appl. Phys. **91**(9), 5533–5537 (2002).
[21] N. Tabatabaie, M. H. Meynadier, R. E. Nahory, J. P. Harbison, and L. T. Florez, "Large lateral photovoltaic effect in modulation-doped Algaas/Gaas heterostructures," Appl. Phys. Lett. **55**(8), 792–794 (1989).
[22] Thorlabs.de., "IR Photoconductive Detectors," see http://www.thorlabs.de/newgrouppage9.cfm?objectgroup_id=6479.
[23] G. Papp and F. M. Peeters, "Resistance maps for a submicron Hall electrosensor in the diffusive regime," J. Appl. Phys. **101**(11), 113717 (2007).
[24] J. R. Dixon and J. K. Furdyna, "Measurement of the static dielectric-constant of the Insb lattice via gyrotropic sphere resonances," Solid State Commun. **35**(2), 195–198 (1980).
[25] S. Zollner, C. T. Lin, E. Schonherr, A. Bohringer, and M. Cardona, "The dielectric function of Alsb from 1.4-Ev to 5.8-Ev determined by spectroscopic ellipsometry," J. Appl. Phys. **66**(1), 383–387 (1989).
[26] Y. A. Pashkin, Y. Nakamura, and J. S. Tsai, "Room-temperature Al single-electron transistor made by electron-beam lithography," Appl. Phys. Lett. **76**(16), 2256–2258 (2000).
[27] R. K. Rajkumar, A. Manzin, D. C. Cox, S. R. P. Silva, A. Tzalenchuk, and O. Kazakova, "3-D mapping of sensitivity of graphene Hall devices to local magnetic and electrical fields," IEEE Trans. Magn. **49**(7), 3445–3448 (2013).
[28] R. K. Rajkumar, A. Asenjo, V. Panchal, A. Manzin, O. Iglesias-Freire, and O. Kazakova, "Magnetic scanning gate microscopy of graphene Hall devices (invited)," J. Appl. Phys. **115**(17), 172606 (2014).
[29] C. C. Tang, M. Y. Li, L. J. Li, C. C. Chi, and J. C. Chen, "Characteristics of a sensitive micro-Hall probe fabricated on chemical vapor deposited graphene over the temperature range from liquid-helium to room temperature," Appl. Phys. Lett. **99**(11), 112107 (2011).
[30] V. Panchal, K. Cedergren, R. Yakimova, A. Tzalenchuk, S. Kubatkin, and O. Kazakova, "Small epitaxial graphene devices for magnetosensing applications," J. Appl. Phys. **111**(7), 07E509 (2012).
[31] M. Bando, T. Ohashi, M. Dede, R. Akram, A. Oral, S. Y. Park, I. Shibasaki, H. Handa, and A. Sandhu, "High sensitivity and multifunctional micro-Hall sensors fabricated using InAlSb/InAsSb/InAlSb heterostructures," J. Appl. Phys. **105**(7), 07E909 (2009).
[32] J. Ferrer, C. J. Lambert, V. M. Garcia-Suarez, D. Z. Manrique, D. Visontai, L. Oroszlany, R. Rodriguez-Ferradas, I. Grace, S. W. D. Bailey, K. Gillemot, H. Sadeghi, and L. A. Algharagholy, "GOLLUM: A next-generation simulation tool for electron, thermal and spin transport," New J. Phys. **16**, 093029 (2014).
[33] M. Buttiker, "4-terminal phase-coherent conductance," Phys. Rev. Lett. **57**(14), 1761–1764 (1986).
[34] H. Sadeghi, S. Sangtarash, and C. J. Lambert, "Enhancing the thermoelectric figure of merit in engineered graphene nanoribbons," Beilstein J. Nanotechnol. **6**, 1176–1182 (2015).
[35] H. Sadeghi, J. A. Mol, C. S. Lau, G. A. D. Briggs, J. Warner, and C. J. Lambert, "Conductance enlargement in picoscale electroburnt graphene nanojunctions," Proc. Natl. Acad. Sci. U.S.A. **112**(9), 2658–2663 (2015).

This article is copyrighted as indicated in the article. Reuse of AIP content is subject to the terms at: http://scitation.aip.org/termsconditions. Downloaded to IP: 148.88.176.132 On: Mon, 14 Dec 2015 11:14:40